JOURNAL OF GEOPHYSICAL RESEARCH, VOL. 115, D08202, doi:10.1029/2009JD013088, 2010

Click Here for Full Article

Estimation of the microphysical aerosol properties over Thessaloniki, Greece, during the SCOUT-O_3 campaign with the synergy of Raman lidar and Sun photometer data

D. Balis,[1] E. Giannakaki,[1] D. Müller,[2] V. Amiridis,[3] K. Kelektsoglou,[4] S. Rapsomanikis,[4] and A. Bais[1]

Received 27 August 2009; revised 24 November 2009; accepted 2 December 2009; published 23 April 2010.

[1] An experimental campaign was held at Thessaloniki, Greece (40.6°N, 22.9°E), in July 2006, in the framework of the integrated project Stratosphere-Climate Links with Emphasis on the Upper Troposphere and Lower Stratosphere (SCOUT-O_3). One of the main objectives of the campaign was to determine the local aerosol properties and their impact on the UV irradiance at the Earth's surface. In this article, we present vertically resolved microphysical aerosol properties retrieved from the inversion of optical data that were obtained from a combined one-wavelength Raman/two-wavelength backscatter lidar system and a CIMEL Sun photometer. A number of assumptions were undertaken to overcome the limitations of the existing optical input data needed for the retrieval of microphysical properties. We found acceptable agreement with Aerosol Robotic Network retrievals for the fine-mode particle effective radius, which ranged between 0.11 and 0.19 for the campaign period. It is shown that under complex layering of the aerosols, general assumptions may result in unrealistic retrievals, especially in the presence of aged smoke aerosols. Furthermore, with this instrument setup, the inversion algorithm can also be applied successfully for the complex refractive index in cases of vertically homogeneous layers of continental polluted aerosols. For these inversion cases, the vertically resolved retrievals for the single-scattering albedo resulted in values around 0.9 at 532 nm, which were in very good agreement with estimates from airborne in situ observations obtained in the vicinity of the lidar site.

Citation: Balis, D., E. Giannakaki, D. Müller, V. Amiridis, K. Kelektsoglou, S. Rapsomanikis, and A. Bais (2010), Estimation of the microphysical aerosol properties over Thessaloniki, Greece, during the SCOUT-O_3 campaign with the synergy of Raman lidar and Sun photometer data, *J. Geophys. Res.*, *115*, D08202, doi:10.1029/2009JD013088.

1. Introduction

[2] Atmospheric aerosols have a strong influence on radiative forcing, chemical processes in the atmosphere, cloud properties, and air quality [*Solomon et al.*, 2007]. The occurrence, residence time, physical properties, chemical composition, and corresponding complex refractive index characteristics of the particles, as well as the resulting climate-relevant optical properties are subject to large diversity, especially in the troposphere, due to widely different sources and meteorological processes. Despite their importance in atmospheric physics, significant gaps in the scientific knowledge about aerosols still exist. This lack of knowledge is particularly true for the vertical distribution of aerosols in the atmosphere, which is of essential relevance to understanding aerosol effects on climate [e.g., *Kaufman and Fraser*, 1997]. Thus, systematic observations of acceptable accuracy of vertical profiles of the physical and optical properties of the particles are needed for the characterization of aerosol distribution and properties, such as the particle surface area concentration, volume and mass concentrations, mean particle size, and volume extinction coefficient. These parameters can only be retrieved by ground-based multi-wavelength lidars, directly, concerning the extinction and backscatter profiles and by the application of advanced retrieval algorithms on the optical data for the retrieval of microphysical properties.

[3] Ground-based remote sensing of particles is a cornerstone to aerosol monitoring, and, in particular, the establishment of monitoring networks has generated significant progress over the past 10 years. Routine monitoring of particle optical properties has been carried out in the framework of networks (e.g., the Aerosol Robotic Network (AERONET) [*Holben et al.*, 1998] and the European Aerosol Research

[1]Laboratory of Atmospheric Physics, Aristotle University of Thessaloniki, Thessaloniki, Greece.
[2]Leibniz Institute for Tropospheric Research, Leipzig, Germany.
[3]Institute for Space Applications and Remote Sensing, National Observatory of Athens, Athens, Greece.
[4]Department of Environmental Engineering, Democritus University of Thrace, Xanthi, Greece.

Copyright 2010 by the American Geophysical Union.
0148-0227/10/2009JD013088

Lidar Network (EARLINET) [*Bösenberg et al.*, 2003]). Advanced retrieval algorithms for microphysical aerosol properties have been developed in the framework of these networks [e.g., *Dubovik and King*, 2000; *Müller et al.*, 1999a, 1999b]. AERONET stations provide inversion-based retrievals of a variety of effective, column-mean properties such as size distributions, phase function, asymmetry factor, and single-scattering albedo [*Dubovik and King*, 2000]. It should be noted, however, that even if these data have been widely used for aerosol studies, the inversion-based retrieval products have yet to be systematically validated by comparison to in situ measurements. Yet, EARLINET stations use the Raman lidar technique with increasing sophistication to demonstrate robust retrievals of microphysical parameters (effective radius, complex index of refraction, and single-scattering albedo) along with the backscatter and extinction profiles. *Müller et al.* [1999a, 1999b, 2001] and *Veselovskii et al.* [2002] have demonstrated this capability using multiwavelength elastic/Raman backscatter lidar systems. The algorithm has been applied in several aerosol studies [e.g., *Müller et al.*, 2005, 2006; *Tesche et al.*, 2008] and has been tested in intensive field campaigns (e.g., during Indian Ocean Experiment (INDOEX) [*Müller et al.*, 2003] and Aerosol Characterization Experiment 2 (ACE 2) [*Müller et al.*, 2002]). However, and similar to the AERONET case, the inversion-based retrievals of this method have to be systematically validated against in situ (preferably aircraft for lidar case) data. Because aircraft data are not frequently available, such studies are usually restricted during field campaigns.

[4] From 12 to 25 July 2006, a UV-aerosol campaign took place in Thessaloniki, Greece, as part of the integrated project Stratosphere-Climate Links with Emphasis on the Upper Troposphere and Lower Stratosphere (SCOUT-O_3). One of the goals of the campaign was to investigate how changes in aerosol affect UV levels at the ground and to derive parameterizations of the aerosol properties from radiation measurements by comparison with in situ and remote-sensing aerosol measurements. The campaign was organized at Thessaloniki, Greece, a location with high aerosol load and high probability of day-to-day aerosol variations, and of alternating clear and cloudy days. The measurements at ground level were carried out by several spectroradiometers, Sun photometers, and other radiation instruments, as well as a suite of in situ aerosol instrumentation for measuring their composition and optical properties. Two aircrafts were also used to measure the optical, physical, and chemical properties of the aerosols at different altitudes in the greater area of Thessaloniki. Finally, aerosol load was continuously monitored by a CIMEL Sun photometer (part of the AERONET) and a combined UV Raman/backscatter lidar (part of the EARLINET). Selected well-focused studies were performed for the physical characterization of aerosol load by applying microphysical retrieval inversion algorithms on CIMEL and lidar data.

[5] The article is organized as follows. In section 2, the Raman lidar, Sun photometer, and aircraft instruments are presented, along with a brief description of the inversion algorithm and application problems. In section 3, we present inversion results for the SCOUT-O_3 campaign period. Section 4 closes with summary and concluding remarks.

2. Data and Methodology

2.1. Lidar Data

[6] At the Laboratory of Atmospheric Physics of the Aristotle University of Thessaloniki (LAP-AUTH), a two-wavelength combined Raman elastic-backscatter lidar has been used since 2001 [e.g., *Balis et al.*, 2004; *Amiridis et al.*, 2005] to perform continuous measurements of suspended aerosols particles in the planetary boundary layer (PBL) and the lower free troposphere (FT). The LAP-AUTH lidar is based on the second and third harmonic frequency of a pulsed Nd:YAG laser, which emits pulses of 300 and 120 mJ output energy at 532 and 355 nm, respectively, with a 10 Hz repetition rate. The optical receiver is a 500 mm diameter Newtonian telescope with 0.7–3 mrad adjustable field of view. Three Hamamatsu R7400P-06 photomultipliers are used to detect the lidar signals at 532, 355, and 387 nm with 15 m height resolution and 2 min time resolution. The lidar system of LAP and the algorithms implemented were successfully intercompared in the frame of the EARLINET [*Matthias et al.*, 2004; *Böckmann et al.*, 2004; *Pappalardo et al.*, 2004].

2.2. Sun Photometer Data

[7] The Sun photometer observations reported in this article were performed by a CIMEL Sun-sky radiometer, which is part of the AERONET Global Network (http://aeronet.gsfc.nasa.gov). The CIMEL of Democritus University of Thrace was installed at Thessaloniki in June 2003. The CIMEL is an automatic Sun-sky scanning filter radiometer that allows the measurements of the direct solar irradiance and sky radiance at wavelengths 340, 380, 440, 500, 670, 870, and 1020 nm. The technical specifications of the instrument are given in detail by *Holben et al.* [1998]. In this article, we used level 2 data for the optical properties and level 1.5 data for the retrieval of the microphysical properties of the aerosols.

2.3. Aircraft Measurements

[8] The aircraft instrumentation used during the SCOUT-O_3 campaign was installed on the modified Cessna 310 aircraft of the Democritus University of Thrace. Aerosol scattering coefficient measurements were carried out using a Radiance Research model M903 Integrating Nephelometer. Aerosol light absorption coefficient was measured with a sampling frequency of 1 Hz at 565 nm with a Radiance Research filter-based Particle Soot/Absorption Photometer (PSAP). The data from the PSAP were corrected using the corrections given by *Bond et al.* [1999]. A GPSMAP 195 (Garmin) was used to provide three-dimensional location information (latitude, longitude, altitude, World Geodetic System 84) of the aircraft at 1 Hz sampling frequency. The combination of aerosol total scattering and absorption coefficient measurements was used for the determination of aerosol light extinction coefficient, single-scattering albedo, and the aerosol optical depth (AOD). Flights included several patterns to sample different regions of the lower troposphere and circles at several altitudes to quantify the vertical mixing of aerosol. Four flights were performed over

Thessaloniki in July 2006. In this study, we use the two of them to validate the results of the inversion algorithm used to determine the single-scattering albedo of aerosols. Specifically, the two flights were carried out in the afternoons of 18 and 19 July 2006. The first flight took place at 18 July 2006 between 1715 and 1814 LT, starting from 40.31°N and 22.57°E and ending at 40.34°N and 22.58°E, while the second flight performed at 19 July 2006 between 1700 and 1837 LT, starting from 40.31°E and 22.58°E and ending at the geographic point of 40.31°N and 22.58°E. The aircraft was flown at low altitude patterns to allow measurements of aerosol particles within the boundary layer. Every flight pattern included three circles at three different altitudes (350 m, 1000 m, 2500 m) during the ascent. The first two sampling levels were conducted at 350 and 1000 m because of air flight control restrictions. The third one, at 2500 m, was conducted at a flight level above the PBL. Measurements at each height lasted 17–20 min. A complete description of instrumentation and flights of the aircraft during the SCOUT-O_3 campaign is given by *Kelektsoglou et al.* [2010].

2.4. Inversion Algorithm and Application Problems

[9] Microphysical particle properties are derived with an inversion algorithm that has been developed at the Leibniz Institute for Tropospheric Research (IfT). A detailed description of the inversion code is given by *Müller et al.* [1999a, 1999b]. Modifications concerning the selection of the optimum solution space were made by *Veselovskii et al.* [2002]. Changes concerning the minimum number of measurement wavelengths that are needed for the inversion are given by *Müller et al.* [2001] and *Veselovskii et al.* [2002]. The most critical conclusion of these studies is that only the combined use of particle backscatter and extinction coefficients in the inversion algorithm can provide acceptable accurate results for the particle size distribution as well as the complex refractive index. This information can then be used to calculate the particle single scattering albedo with a Mie scattering code [e.g., *Bohren and Huffman*, 1983]. Previous simulation studies, showing acceptable accurate results, used particle backscatter coefficients at a minimum of three wavelengths (355, 532, and 1064 nm) and extinction measurements at two wavelengths (355 and 532 nm), whereas the measurement errors on average should be <20%. Uncertainties on the retrievals are in general <30% for effective radius. Errors can become as large as 50% for volume and surface area concentration. The real part of the complex refractive index is derived with an accuracy of better than ±0.1. The imaginary part is found to its correct order of magnitude, if it is <0.01*i*. For larger values of the imaginary part, the uncertainty is <50%. The single scattering albedo can be calculated with an accuracy of ±0.05, if uncertainties of the input optical data on average are <10–15%. A detailed error analysis is given by *Müller et al.* [1999b, 2001] and *Veselovskii et al.* [2002, 2004].

[10] In recent years, simulation studies have been carried out to investigate whether a combination of data from Raman lidar (backscatter and extinction coefficients) and sun photometer (optical depth and thus extinction coefficients) can also be used for the retrieval of microphysical particle properties with the inversion algorithm of IfT [e.g., *Tesche et al.*, 2008; *Pahlow et al.*, 2006]. *Pahlow et al.* [2006] performed computer simulations and found that the use of three to five Sun photometer channels, evenly distributed in the wavelength range from 300 to 1100 nm, are enough to derive the investigated particle size parameters with an average accuracy of 30%, if at the same time backscatter coefficients at two wavelengths are used. *Tesche et al.* [2008] and *Müller et al.* [2006] subsequently analyzed data from a combination of sun photometer and a one-wavelength Raman lidar (backscatter and extinction coefficients at 532 nm). In this article, we extend the previous studies to data sets that contain Raman lidar measurements of one extinction coefficient (355 nm) and two backscatter coefficients (355 and 532 nm) and Sun photometer data, in addition to a large number of in situ aerosol-related measurements at the surface and on the aircraft available in the frame of the SCOUT-O_3 campaign.

[11] We could basically follow the approach of data analysis outlined by *Pahlow et al.* [2006]. However, in our specific case, we had to deal with several deficiencies in the available data sets. We had to make a number of critical assumptions on the data to come up with the minimum combination of data (backscatter and extinction coefficients) that according to the previous discussion, are needed to carry out an accurate inversion. The optical data needed as input to our inversion algorithm are profiles of the extinction coefficients at 355, 532, and 1020 nm, in combination with profiles of the backscatter coefficients at 355 and 532 nm. As mentioned previously, in our experimental setup, we have fewer vertically resolved optical data from lidar, namely, the backscatter coefficients at 355 and 532 nm and the extinction coefficient at 355 nm. To come up with the optimum data set needed for the inversions, we followed three assumptions that are presented in the following:

2.4.1. First Assumption: Consistency of Daytime Sun Photometric and Nighttime Lidar Optical Data

[12] First, to upgrade our limited vertically resolved optical data, we used column-averaged optical depth information that we obtained from Sun photometric measurements. To do that, we have to assume that daytime Sun photometric and nighttime lidar data are referring to the same aerosol burden. The validity of this assumption is examined before the inversion application, and an example of our tests is presented in section 3.1.

2.4.2. Second Assumption: Equality of the Lidar Ratios at 355 and 532 nm

[13] For the calculation of the extinction coefficient profile at 532 nm, we hypothesize that the lidar ratios at 355 and 532 nm are equal. Knowing the backscatter coefficients at 355 and 532 nm and the extinction coefficient at 355 nm, it is possible under the lidar ratio equality assumption to retrieve the extinction coefficient profile at 532 nm. However, the lidar ratio equality at 355 and 532 nm is a highly uncertain hypothesis, and it is examined in section 3.2.

2.4.3. Third Assumption: Equality of the Layer-to-Columnar Ratio of the Angstrom Spectral Dependence

[14] For the calculation of the extinction coefficient at 1020 nm in specific height layers, we first calculate the ratio of the extinction-related angstrom exponent in a predefined layer (estimated from the lidar measurements) to the columnar angstrom exponent between wavelengths in the UV (355 nm) and visible light spectrometer (VIS) (532 nm) spectral region (estimated from the Sun photometer). Then

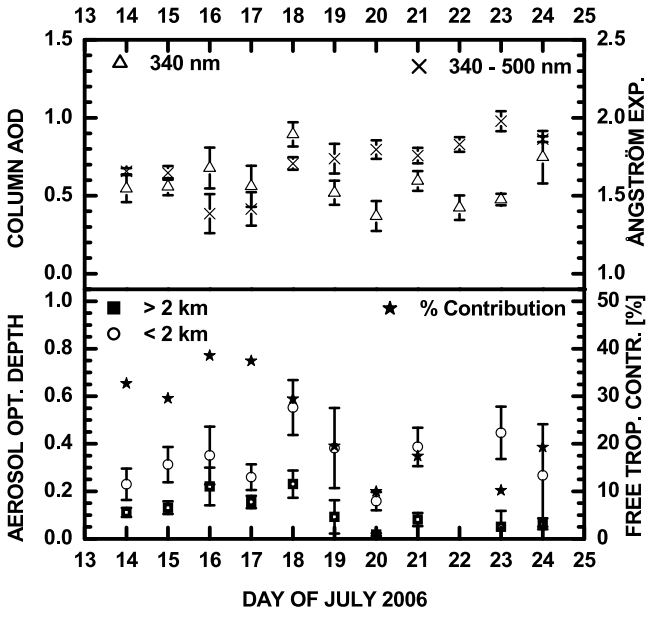

Figure 1. (top) Aerosol optical depth (380 nm) and angstrom exponent (380/500 nm) at Thessaloniki, Greece, for July 2006, based on Sun photometer data. (bottom) Integrated aerosol extinction at 355 nm for heights below and above 2 km based on Laboratory of Atmospheric Physics of the Aristotle University of Thessaloniki (LAP-AUTH) lidar data and the corresponding percentage of free troposphere (FT) aerosol contribution to the total aerosol optical depth (AOD).

we assume that this ratio is the same with the corresponding ratio between the VIS (532 nm) and IR (1020 nm) spectral region, keeping in mind that we can also estimate the columnar angstrom exponent between VIS and IR from the Sun photometer. In this way, and already knowing the extinction coefficient at 532 nm from the second assumption, we can estimate from equation (1) an extinction profile at 1020 nm:

$$\frac{A^{\text{layer}}_{355/532}}{A^{\text{column}}_{355/532}} = \frac{A^{\text{layer}}_{532/1020}}{A^{\text{column}}_{532/1020}} \tag{1}$$

3. Results and Discussion

[15] During the SCOUT-O_3 UV campaign, the aerosol burden over Thessaloniki experienced large variations in load and nature, mainly due to the variable prevailing meteorological conditions, which resulted in the advection of air masses from different sources. In addition, different local pollution events were observed during this 10 day period. Figure 1 (top) presents the daily mean columnar AOD values at 340 nm during the campaign, as these were observed with the CIMEL Sun photometer, and the corresponding daily mean angstrom exponent calculated in the 340–500 nm wavelength region. The AOD ranged from 0.3 to almost 1, whereas the angstrom exponent varied between 1.3 and 2, also indicating a large variability in the size of the aerosol load over Thessaloniki. To estimate the contribution of light extinction by free tropospheric particles to the total tropospheric optical depth during the campaign period, we calculated the AOD in the PBL and the FT separately using our lidar measurements and following the approach of *Amiridis et al.* [2005]. For the calculation of the integrated aerosol extinction from daily profiles of the particle backscatter coefficient, we calculated the column-integrated particle backscatter coefficient above and below 2 km, multiplied, when available, with the lidar ratio estimated with the Raman lidar nighttime measurements of the same day or with a lidar ratio estimated from climatological data on the lidar ratio observed with Raman lidar at Thessaloniki [*Amiridis et al.*, 2005], which mainly depends on the origin of the air masses observed. Our results, presented in Figure 1 (bottom), indicate two distinct periods during the campaign: one with high aerosol load in the FT, where the FT contribution to the total AOD is more than 30%, and associated with smaller angstrom exponents, and one period with high aerosol loading in the PBL, where the FT contribution is less than 20%. AOD at 550 nm was also estimated from the aircraft data by adding and integrating the nephelometer and PSAP data from the ground up to 2500 m. The AOD estimated from the aircraft also confirms this day-to-day variability; however, due to their small vertical extent (0−2500 m), the aircraft data underestimate systematically both AERONET and lidar AOD estimates [*Kelektsoglou et al.*, 2010].

[16] For the period of the SCOUT-O_3 campaign, we estimated profiles of the effective radius, the refractive index, and the single-scattering albedo for 3 days (16, 18, and 19 July 2006) on which the application of the inversion algorithm was possible, according to the criteria discussed in section 2.4. In the next paragraph, we examine in detail the case of 16 July 2006. First, we demonstrate the approach we followed for the estimation of the microphysical properties using synergistically lidar and Sun photometric measurements, which was presented in the previous section. Second, we discuss in detail the retrieval results for the observed layers. The same approach was also applied to the other 2 days, and the results are presented and discussed in section 3.2.

3.1. Case Study of 16 July 2006: A Complex Profile

[17] To derive the microphysical properties at different altitudes, the lidar profiles have to be separated into distinct aerosol layers. The segregation of the lidar profiles was based on the concept that each layer should be characterized by distinguishable and relatively stable optical properties, which means that within a chosen height layer, the variability of the optical data should be less than the statistical uncertainty of the individual data points. Mean values of optical properties calculated within the defined layers were then used as input in the inversion algorithm, following the assumptions discussed in section 2.4. The required homogeneity of an aerosol layer is hypothesized from the lack of variability of the lidar ratio and/or backscatter-related angstrom exponent within the height range of the layer. Figure 2 shows the lidar profiles measured around 1900 UT on 16 July 2009 at Thessaloniki, and the horizontal lines outline the defined layers. As shown in Figure 2, both the extinction and backscatter profiles showed an increase below 1 km, associated with local emission within the PBL

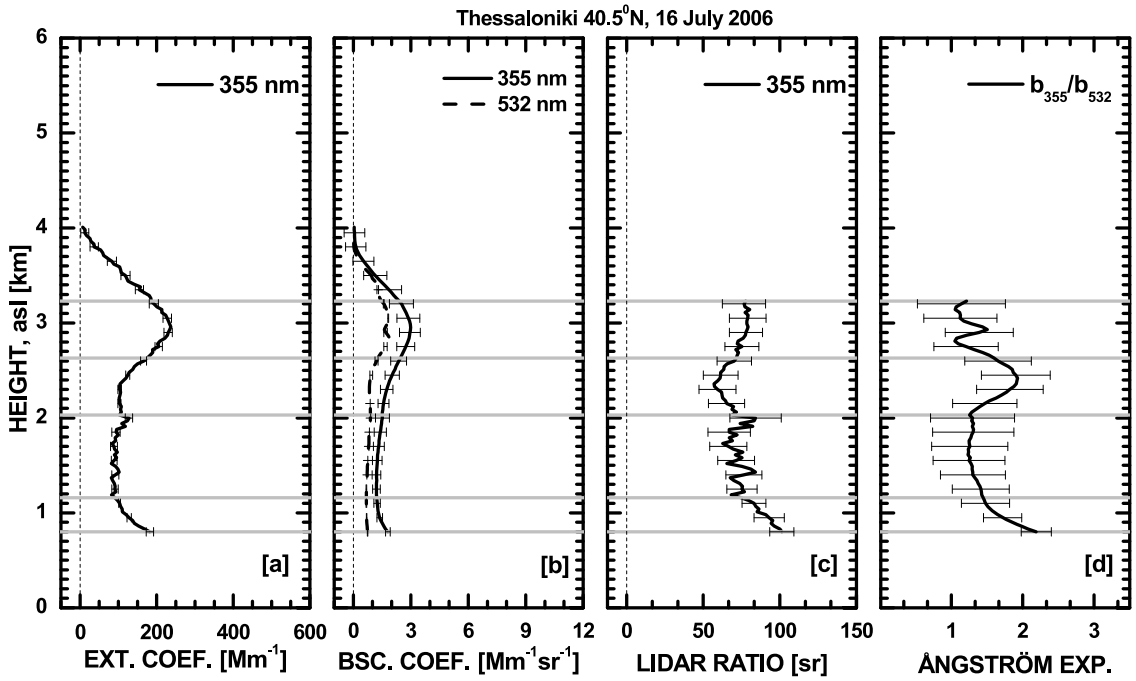

Figure 2. Extinction and backscatter coefficients, corresponding lidar ratio, and backscatter-related angstrom exponent on 16 July 2006 at 1845 UTC.

and a distinct layer at 3 km discussed in the next paragraph. The integrated AOD above the complete overlap (here around 0.8 km) was 0.4, indicating a relative polluted day compared to climatological values for Thessaloniki [*Kazadzis et al.*, 2007; *Amiridis et al.*, 2005]. The mean lidar ratio of 75*sr* and the mean backscatter-related angstrom exponent of 1.44 indicate the presence of polluted continental aerosols in the area; however, details on the potential sources and aerosol types are discussed in the next paragraph.

[18] To synergistically use the Sun photometer data for the estimation of the input optical data to the inversion model, we have to assure that the aerosol variability between the afternoon Sun photometer data and the sunset lidar measurements is not significant. For the case of 16 July 2006, this stability is demonstrated in Figure 3, where it is evident that AOD (at 380 nm) and angstrom (380–500 nm) variability is not significant after 1500 UTC. In addition, according to the last Sun photometric measurements at around 1600 UT, both parameters are in agreement with the lidar estimations at around 1900 UT. AOD from lidar measurements was calculated by integrating the extinction coefficient at 355 nm in the atmospheric column, assuming that the calculated extinction value at the lowest height of the complete overlap is representative for the incomplete overlap region. Lidar-derived angstrom exponents in Figure 3 were calculated by the backscatter coefficients at 355 and 532 nm (the so-called backscatter-related angstrom exponent).

[19] After checking the consistency of daytime Sun photometric and nighttime lidar data, we applied the assumptions described in section 2.4 for each of the layers determined in Figure 2 to estimate, with the synergy of lidar and sun photometer, the optical data for each layer needed as input to the inversion code. For each layer, we applied the inversion algorithm to the mean values of our optical data to estimate the effective radius from the whole size distribution, the effective radius for the fine mode (particles smaller than 1 μm in radius), the real and imaginary part of the refractive index, and the single-scattering albedo at 532 nm. The retrieved profiles are shown in Figure 4. Figure 4 (left) indicates vertical homogeneous conditions concerning the effective radius of the fine mode and the absence of a coarse mode in the

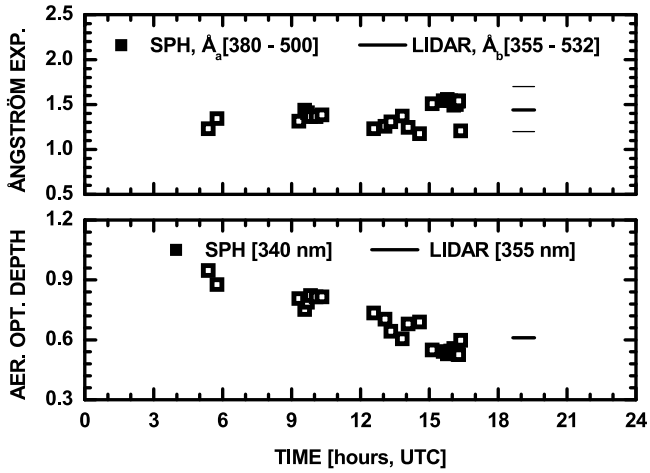

Figure 3. Aerosol optical depth (AOD) at 380 nm and extinction-related angstrom exponent (380/500 nm) from Sun photometer measurements (open squares), as well as AOD at 355 nm and backscatter-related angstrom exponent (355/532 nm) from lidar measurements (thin lines) for 16 July 2006.

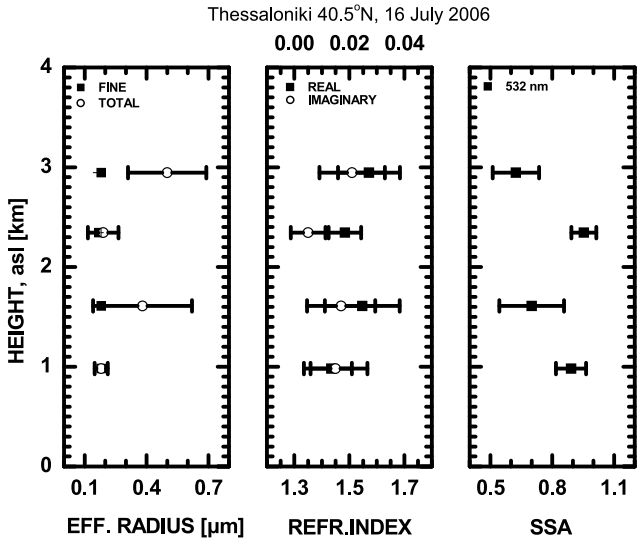

Figure 4. Estimated profiles of the effective radius, refractive index, and single-scattering albedo at Thessaloniki for 16 June 2006.

inversion estimates at 1 and 2.5 km (first and third layers, respectively). However, there are two layers at around 1.5 and 3 km where the inversion estimates a significant contribution from coarse-mode particles. Before analyzing in detail the estimated vertical structures, we should consider that during the time window of the lidar measurements, scattered clouds at 3 km were occasionally present above the measuring site. Lidar measurements contaminated with clouds have been excluded from our analysis. To interpret the inverted properties for these four layers, we used 10-day back trajectories calculated with NOAA HYSPLIT model [*Draxler and Hess*, 1998], which provides us with some information on the origin of the observed air masses (Figure 5, top).

[20] In the first layer at approximately 1 km, the retrieved total effective radius was 0.18 μm. The retrieved size distribution did not show particles larger than 1 μm, and therefore, the effective radius of the fine mode was almost equal to the total one. The single-scattering albedo within this layer was estimated to 0.89. This was due to the relatively small values of the imaginary part of the refractive index (0.015*i*). These relatively small (in size) and moderate absorbing particles were more likely associated with sources within the PBL. As seen from the trajectory calculations in Figure 5 (top), the air masses arriving at Thessaloniki at 1 km could be affected by aerosol pollution advected from the north but, eventually, not significantly because this northerly flow was characterized by a catabatic motion in the vertical. Similar air mass flows are also observed for the second layer under study at 1.6 km, and because the local PBL anthropogenic pollution is not likely to be present at those altitudes, we consider the aerosol burden for this layer as continental polluted. The total effective radius of 0.38 μm estimated for this layer, however, was much larger compared with studies where anthropogenic European pollution was observed [e.g., *Müller et al.*, 2002]. According to this study for anthropogenic European pollution, the estimated effective radius ranges between 0.08 and 0.31 μm, whereas the estimated mean single-scattering albedo is of the order of 0.95 ± 0.06 at 532 nm. Comparing the reported values with our inversion results (total effective radius of 0.38 μm and single-scattering albedo of 0.7 at 532 nm), we conclude that if the aerosol type is common with the previously mentioned studies (as we hypothesize from the trajectory analysis), the application of the inversion algorithm for the second layer is not realistic.

[21] For the third layer at 2.3 km, trajectory analysis showed that the air masses originate from areas of northern Canada where forest fires were observed from satellite sensors (ATSR World Fire Atlas). This indicates that the observed layer was associated with the presence of aged smoke particles. However, the retrieved value of the effective radius of 0.19 μm was smaller than the ones estimated for aged smoke from previous studies (Figure 9). For example, *Müller et al.* [2005] reported effective radius for aged smoke between 0.24 and 0.41 μm.

[22] Finally, for the fourth layer under study at 2.9 km, back trajectories indicate negligible aerosol advection from remote sources. The large total effective radius of 0.5 found for this layer results from the secondary coarse-mode maximum in the volume size distribution revealed from the inversion. If we consider the existence of scattered clouds at heights above 2.5 km and also examine the relative humidity profile measured just a few kilometers far from the lidar station (shown in Figure 5 (top)), which shows a very humid layer (relative humidity close to 100%) in the 2.5–4 km region, we can attribute this coarse mode to the contribution of the "tail" of the scattered clouds in our lidar measurements. *Veselovskii et al.* [2004] also found large values of the total effective radius when studying the microphysical properties of anthropogenic aerosols in the presence of clouds.

[23] For the presented case study of 16 July 2006, inversion results may be affected with high uncertainty (more than 50%, as seen later in Figure 6) for layers 2–4. These unrealistic results are mainly attributed to the insufficient optical input data to the inversion algorithm due to the lack of extinction measurements at 532 nm. For the application of the inversion algorithm in the case of Thessaloniki's two-backscatter one-extinction backscatter/Raman lidar, the most critical assumption in our approach is the assumed equality between the lidar ratios at 355 and 532 nm. According to *Müller et al.* [2007], the spectral dependence of the lidar ratio depends mostly on the aerosol type. Collected data presented by *Müller et al.* [2007] showed that the ratio of the lidar ratios measured at 355 and 532 nm for anthropogenic particles in Europe was approximately equal to 1.1. However, the ratio of the lidar ratios for aged smoke particles was found to range between 0.6 and 1.0.

[24] In Figure 6, we present a sensitivity analysis on the results of our inversions based on different assumptions of the ratio of the lidar ratios at 355 and 532 nm. Specifically, we present results for 16 (already presented) and 19 July 2006, a day with more homogeneous layering of the aerosols. Inversion results for the layers defined for both days are presented in Figure 6 in terms of the total (Figure 6, top) and fine (Figure 6, bottom) effective radius and assuming ratios of the lidar ratios at 355 and 532 nm of 0.8, 1.0, and 1.2. The assumption of the ratio becomes more critical for 16 July, especially for the total aerosol effective radius of the second, third, and fourth layers. This large uncertainty in

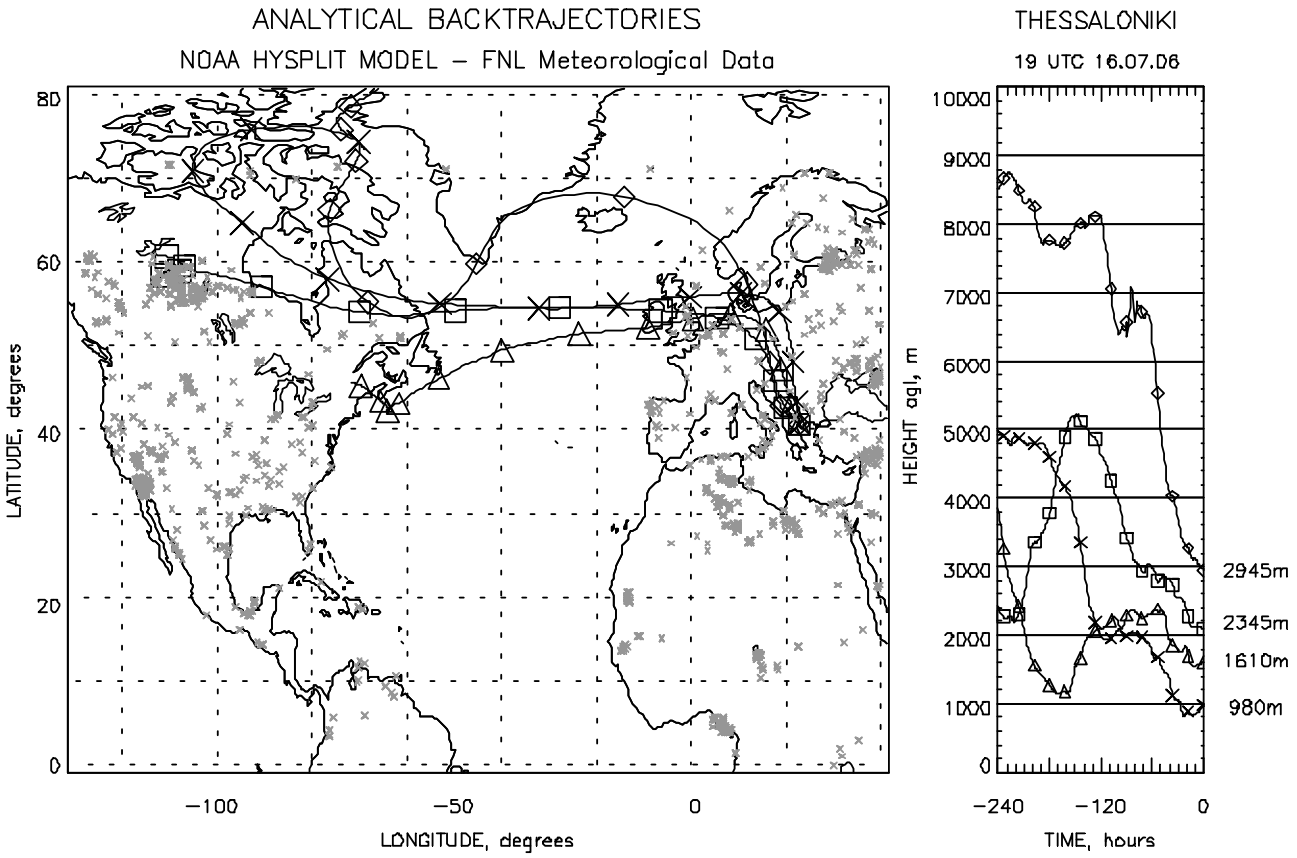

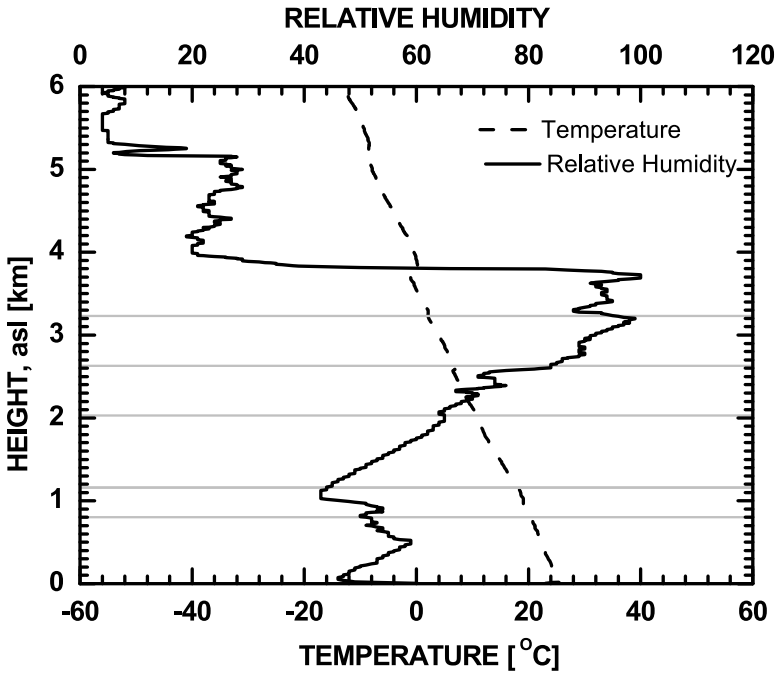

Figure 5. Ten-day back trajectories at Thessaloniki for 16 July 2006 at 19 UTC and locations of fires from the ATSR World Fire Atlas (top). Vertical profiles of the relative humidity and temperature at Thessaloniki Airport for 16 July 2006 at 23:36 UTC (bottom).

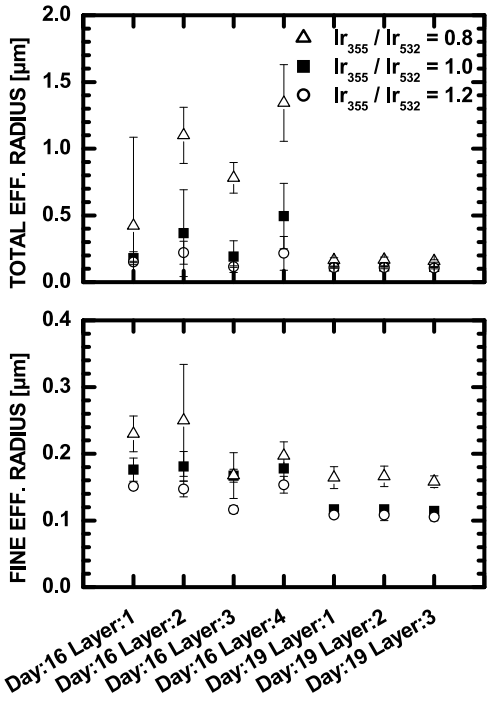

Figure 6. Effect of the different assumption on the ratio of the lidar ratios at 355 and 532 nm for different layers on 16 and 19 July 2006.

the estimation of the total aerosol effective radius for that day is attributed to the existence of secondary modes in the size distribution (aged smokes, water droplets). These modes that can be additionally justified from the trajectory and meteorological analysis indicate that in such complex layering of the aerosols, our assumptions can lead to unrealistic solutions. As evident from Figure 6, larger differences on the inversion results are found when the ratio of the lidar ratios at 355 and 532 nm is assumed to be equal to 0.8. This property feature is more likely characteristic of aged biomass burning particles [*Müller et al.*, 2005], so it applies only for the third layer of 16 August 2006, when smoke particles' presence over Thessaloniki was indicated by the trajectory analysis. Our calculations considering $lr355/lr532 = 0.8$ for this layer result in an effective radius of 0.78, which on the other side is unrealistically large for such types of aerosols. Volume size distributions for this layer (not shown here) revealed a well-defined maximum at 0.12 μm particle radius, which corresponds mostly to aerosols of anthropogenic origin, a broadening of the distribution to radii of 0.3 μm indicating the existence of a second mode, consistent with the presence of smoke particles. However, this assumption leads to model solutions also in the coarse mode, which cannot be attributed to either anthropogenic or smoke particles. On the contrary, for the case of 19 July, the inversion results do not reveal a coarse mode under any different assumptions on the ratio of lidar ratios at 355 and 532 nm. In the next paragraph, we present the case of 18 and 19 July 2006 within the SCOUT-O_3 campaign, where the observed layers do not show large inhomogeneities concerning the aerosol type. For both days when the inversion results were stable, the aerosol burden over Thessaloniki was not characterized by strong layering, and trajectory analysis indicated no significant contribution from remote sources.

3.2. Inversion Retrievals of Vertical Distributions of Effective Radius, Refractive Index, and Single Scattering Albedo and Comparison With In Situ Aircraft Measurements

[25] In Figure 7, we present profiles of the optical and microphysical aerosol properties for 18 and 19 July 2006. In particular, Figure 7 (left) shows profiles of the aerosol extinction coefficient at 355 nm, the backscatter coefficient at 355 and 532 nm, the lidar ratio at 355 nm, and the backscatter-related angstrom exponent. On the basis of these profiles, we determined the layers for which we estimated the microphysical properties, based on the methodology we described in the previous paragraph. For these layers, based on the assumption that $lr355 = lr532$, we show the retrieved total effective radius, the effective radius of the fine mode, the real and imaginary part of the refractive index, and the single-scattering albedo at 532 nm. In addition, we show high-resolution profiles of the single-scattering albedo at 550 nm, based on airborne nephelometer and PSAP measurements [*Kelektsoglou et al.*, 2010].

[26] According to the extinction profiles and the Sun photometric measurements, 18 July was characterized by large optical depths around 0.8 at 340 nm, and the aerosol layers extended up to 4 km, resulting in a FT contribution to the total AOD of about 30%. In addition, the profile is characterized by large extinction-to-backscatter ratio values around 120*sr*. The radiosonde data of the same day shows relative humidity values between 80% and 95% in the 1–3 km layer. Hygroscopic particle growth may be responsible for the observed large lidar ratio values in the same layer [e.g., *Veselovskii et al.*, 2004]. The backscatter-related angstrom exponent indicates the presence of larger particles above 2 km relative to the ones observed later in this article. Inversion-retrieved microphysical properties are shown in Figure 7 (right). The profile indicates the absence of coarse-mode particles since the effective radius of the fine mode and the total effective radius is almost identical for all three layers. The total effective radius is 0.18 in the first layer and increases to 0.23 in the uppermost layer, which is consistent with the profile of the angstrom exponent. Measurements of the size distribution of the number concentration at all flight layers show very small contribution from particles larger than 1 μm [*Kelektsoglou et al.*, 2010] the highest concentrations were found in the lowermost layer (350 m) for particles with radius 0.3 to 0.5 μm, and in addition, they showed in the altitude range around 2 km higher concentrations only for particles with radius larger than 0.5 μm. The latter might explain the estimated small increase of the effective radius with altitude. The estimated values of the real part of the refractive index are close to 1.3, confirming the large contribution of water in the particles. The profile of the single-scattering albedo at 532 nm shows values between 0.9 and 0.8, indicating the presence of mostly continental polluted aerosols. Based on measurements of the chemical composition of the aerosols available during this flight, *Kelektsoglou et al.* [2010] estimated the complex refractive index for 350 and 2500 m altitudes and found values 1.39–0.01*i* and 1.42–0.01*i*, re-

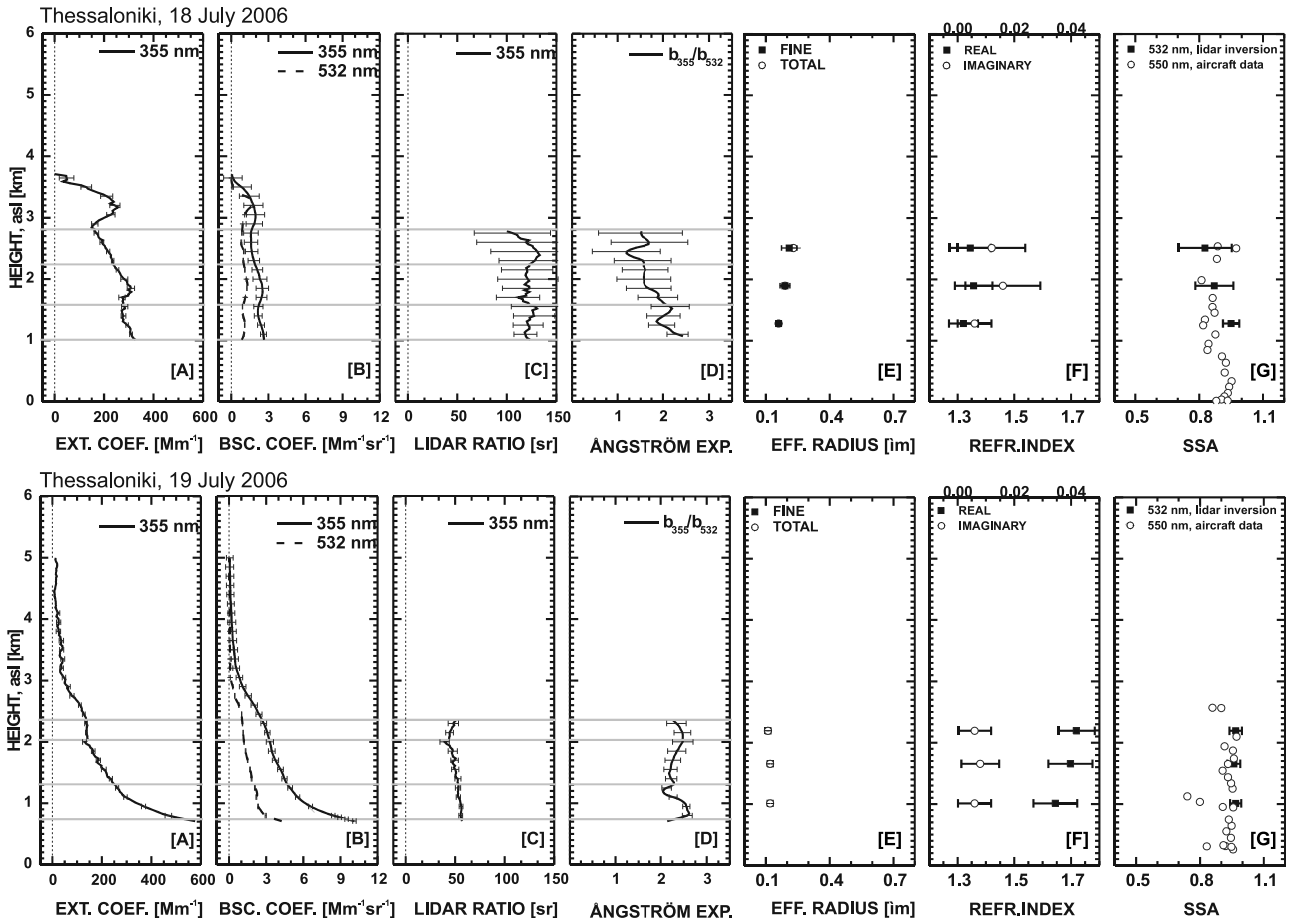

Figure 7. Vertical distribution of (a) aerosol extinction at 355 nm, (b) backscatter at 355 and 532 nm, (c) lidar ratio at 355 nm, and (d) backscatter related Ångström exponent, as estimated from the lidar measurements, (e) vertical distribution of effective radius, (f) refractive index, and (g) single scattering albedo (ω), as estimated from the inversion algorithm (at 532 nm) and air borne in situ (at 550 nm) measurements at Thessaloniki for the 18th of July 2006 (top) and for 19th of July 2006 (bottom).

spectively, which are within the uncertainty of the inversion results.

[27] In Figure 7, we also present the in situ measurements of the single-scattering albedo from the aircraft. The results for the single scattering albedo are in very good agreement with the ones retrieved from the inversion of the lidar data, showing a relative homogeneous layering up to 2.5 km. When examining the effect of our assumption for the lidar ratio at 532 nm ($lr355 = lr532$ versus $lr355/lr532 = 0.8$ and $lr355/lr532 = 1.2$), our results do not change significantly for the total effective radius and the single-scattering albedo. Only the assumption of the $lr355/lr532 = 0.8$, which is indicative for aged smoke (this is not the case here), would result in an overestimation of the fine-mode effective radius.

[28] The 19 July example is typical of continental polluted (anthropogenic) aerosols with a lidar ratio of 50*sr* at 355 nm, which is the average for the season, and backscatter-related angstrom exponent values around 2.1 [*Amiridis et al.*, 2005]. The AOD ranged between 0.5 and 0.6, which is also representative for the season [*Kazadzis et al.*, 2007]. The retrieved microphysical properties show small particles throughout the aerosol layer, with both total and fine-mode effective radius close to 0.12, whereas the real part of the refractive index shows values between 1.65 and 1.72. There were no estimates for the size distribution and the refractive index from the aircraft data for this flight due to problems with the instruments; however, the available data for the atmospheric ionic concentrations indicated the highest values for SO_4^{2+} and Ca^{2+} at heights around 2 km. The estimated refractive index seems to be high to reflect the observed chemical composition but is within the overall large uncertainty of the inversion. The single-scattering albedo was estimated to 0.96 at 532 nm, which is characteristic for moderately polluted continental aerosols. The flight data of 19 July also confirm the retrieved single-scattering albedo values, showing slightly smaller values, however, within the uncertainty of both estimates. The effect of our assumption for the lidar ratio at 532 nm ($lr355 = lr532$ versus $lr355/lr532 = 0.8$ and $lr355/lr532 = 1.2$) produces differences up to 7% in our estimates for the microphysical properties for such homogeneous aerosol conditions, which can be considered small and acceptable, when compared to the 30% accuracy that we inferred from simulation studies [*Pahlow et al.*, 2006].

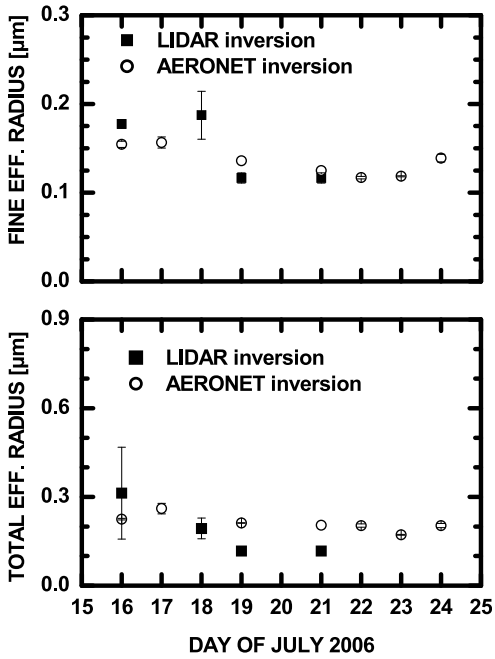

Figure 8. Fine (top) and total (bottom) mean effective radius during the Stratosphere-Climate Links with Emphasis on the Upper Troposphere and Lower Stratosphere (SCOUT-O_3) campaign from Aerosol Robotic Network (AERONET) and lidar inversion results for 16, 18, and 19 July 2006.

3.3. Aerosol Robotic Network Retrieval of Microphysical Properties and Comparison With Lidar Data Inversions

[29] In this section, we present the fine and total effective radius for the SCOUT-O_3 campaign retrieved from level 2 AERONET data. Results from the inversions of lidar data are additionally presented, when available, for comparison in Figure 8. The almucantar inversions of the CIMEL data show that the total effective radius during the campaign period ranged between 0.17 and 0.26 μm, whereas the fine-mode effective radius ranged between 0.11 and 0.16 μm. In all cases of AERONET inversions, the size distributions exhibit a coarse mode, which results in a significant increase of the total effective radius.

[30] When both (lidar and AERONET) inversions are available for the same day, the agreement between the fine-mode effective radii is good, and the observed differences are within 15% for the 2 days, independent of our assumptions for the lidar ratio. The lidar inversion algorithm, however, cannot arithmetically retrieve the coarse modes using the certain optical lidar data as input, and therefore, when comparing the total effective radius, the lidar retrievals underestimate the effective radius by about 40%. For the complex case of 16 July, we show comparisons for the assumption that $lr355 = lr532$ at all layers; however, as already shown in section 3.1, this is not true for all layers, and therefore, the comparison results would highly depend on this assumption.

3.4. Classification of the Aerosols

[31] The retrieved microphysical properties estimated for each layer of the 3 days are compared to lidar inversions from 8 years of data collected by *Müller et al.* [2007]. These data are based both on climatological and campaign data. Certain scatterplots of microphysical properties provide distinct "signatures" for certain types of aerosols, in the case where the sources can be identified. In Figure 9, we show the scatterplot of the volume concentration versus the surface area concentration, the scatterplot of the total effective radius versus the angstrom exponent, and, finally, the scatterplot of the single-scattering albedo at 532 nm versus the imaginary part of the refractive index. The different symbols indicate the average of retrievals based on certain potential aerosol sources regions, respectively, aerosol source mechanisms, and the black circles correspond to the average of the inversions from the SCOUT-O_3 period at Thessaloniki. Our inversion results compare well with the results corresponding to anthropogenic urban pollution in Europe, as determined from measurements performed at other EARLINET stations, showing in addition similarities with cases where anthropogenic pollution coincides with aerosols from forest fires (e.g., INDOEX campaign, special biomass burning events captured in the frame of EARLINET). The large error bars of the mean values shown in these plots indicate that the variability in the aerosol type at Thessaloniki, during the 3 days presented in this study, spans over a wide range of possible aerosol sources, which has been confirmed by trajectories and meteorological observations.

4. Conclusions

[32] We have demonstrated the potential application and limitations of a sophisticated inversion algorithm to lidar data derived from a combined backscatter (two channels)/Raman (one channel) instrument. The feasibility of such an application is important because many lidar systems worldwide have this specific setup. We used an algorithm that was first developed for the routine inversion of backscatter and extinction data from multiwavelength Raman lidar measurements (three backscatter and two extinction channels). To overcome our lidar limitations, we used complementary data from Sun photometric measurements.

[33] There are several reasons that make the combination of extinction data from Sun photometer and backscatter and extinction profiles from lidar a promising new tool for microphysical particle characterization. Profiles of microphysical particle properties can be obtained in many more locations on the globe by lidar/Sun photometer combination, although we must keep in mind that the uncertainty of the derived profiles is likely higher than what is achievable with a multiwavelength (3b + 2a) system alone. In addition, the inversion code itself is an excellent tool to check the consistency and thus the quality of the measured optical data, which are used as input. For instance, if one or more optical input data are wrong (in terms of calibration or large systematic errors), the inversion results would show highly unrealistic values (e.g., for the effective radius).

[34] For anthropogenic pollution, our results for the effective radius of the total particle size distribution and the fine-mode fraction of the size distribution do not change significantly, as long as we vary our assumptions for the ratio of LR_{355} versus LR_{532} within a reasonable range of values. We estimated the effective radius of the fine-mode fraction in the range 0.11 and 0.19 μm. These results are in

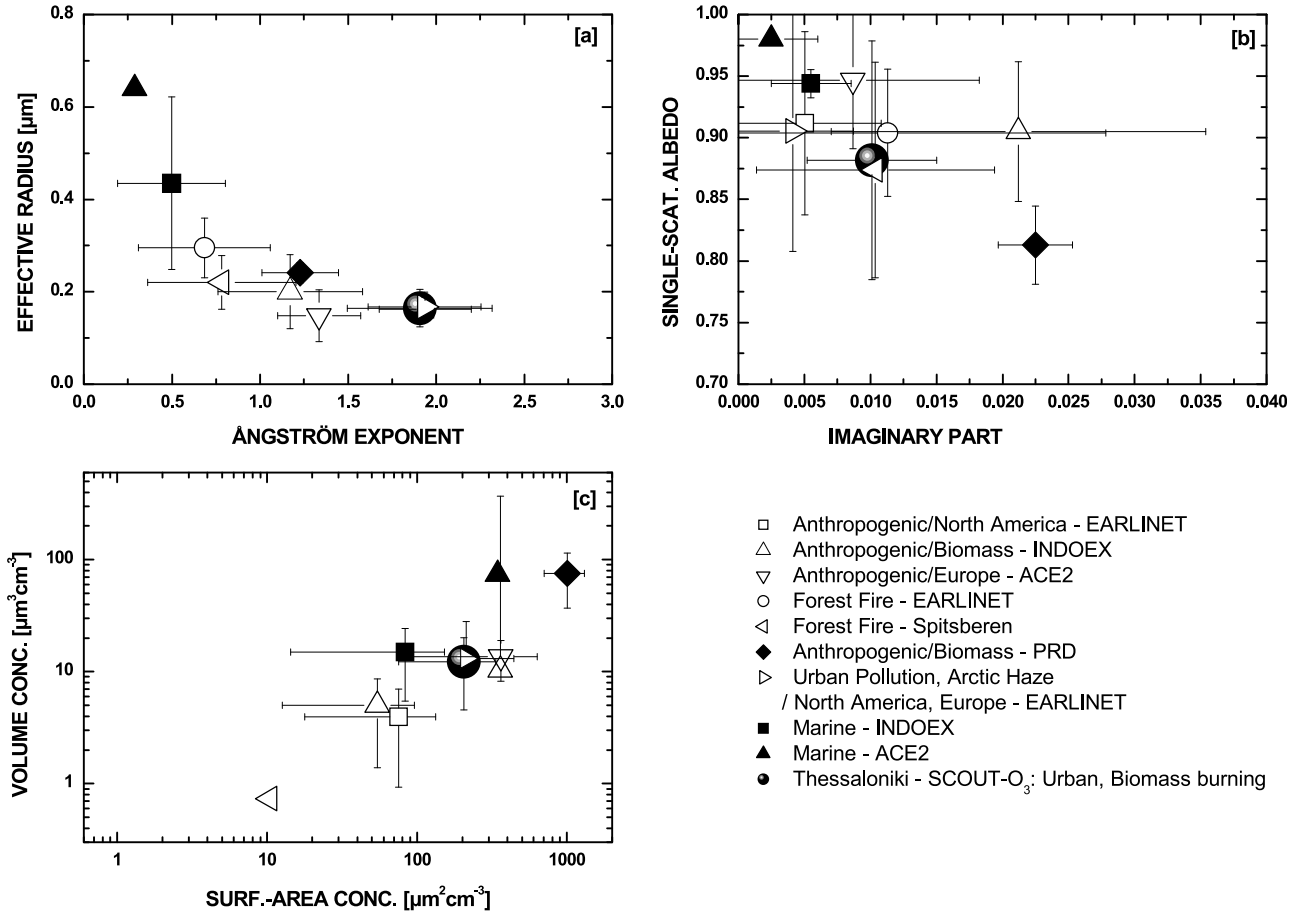

Figure 9. Scatterplots between retrieved microphysical properties for certain aerosol types from lidar optical data: (a) effective radius versus the angstrom exponent, (b) single-scattering albedo at 532 nm versus the imaginary part of the refractive index, and (c) the volume concentration versus the surface area concentration. The different symbols correspond to mean inversions from different campaigns, whereas the open circles correspond to mean inversions from the Stratosphere-Climate Links with Emphasis on the Upper Troposphere and Lower Stratosphere (SCOUT-O_3) campaign at Thessaloniki presented in this study. The error bars correspond to 1σ.

good agreement with AERONET retrievals for the fine mode.

[35] Our approach did not retrieve successfully the coarse mode of the aerosol size distributions because the available measurement wavelengths and optical input data are rather insensitive to coarse-mode particles. Therefore, the total effective radius that is obtained from the AERONET retrieval algorithm is, on average, larger than the total effective radius we obtain from the inversion of the optical data of the lidar/Sun photometer instruments. The inversions were very sensitive to the assumption for the lidar ratio at 532 nm when an aged smoke layer was present in the profile, and in such cases, the inversion could result to unrealistic values for the effective radius. We have to emphasize here, however, that the use of an additional extinction profile (e.g., at 532 nm), measured directly by the lidar as input in the retrieval is crucial and minimizes the need for assumptions, which in complex structures and layers are hard to justify.

[36] For the cases of well-defined, vertically homogeneous anthropogenic pollution, the vertically resolved retrievals for the single-scattering albedo at 532 nm were in good agreement with results from airborne in situ observations, showing values close to 0.95.

[37] The variability of the aerosol type over Thessaloniki during the SCOUT-O_3 campaign allowed us to apply and validate our inversion approach from the synergistic use of lidar and Sun photometric data over a wide range of aerosol sources, which were confirmed by trajectory analysis. Our results were compared to retrieved microphysical properties from lidar inversions collected by *Müller et al.* [2007], based both on climatological and worldwide campaign data, and they were consistent with retrievals that correspond to anthropogenic pollution.

[38] The methodology presented in this article for the retrieval of aerosol microphysical properties, with regard to aerosol type categorization, could be a useful tool for aerosol research. As is shown in this study, certain scatterplots of aerosol microphysical properties may provide distinct "signatures" for certain types of aerosols when the sources can be identified. Such signatures provide a very useful tool to check the quality and consistency of both the optical measurements and the retrieved microphysical properties.

[39] **Acknowledgments.** This work has been conducted in the framework of the projects EARLINET-ASOS under grant RICA-025991 and "SCOUT-O_3" (contract 505390-GOCE-CT-2004) funded by the European Commission. E.G. acknowledges the support of the PENED project (03-ED-344). S.R. thanks the engineers and crew of the DUTH aircraft. The PENED 2003 project is cofinanced: 75% of public expenditure through EC–European Social Fund and 25% of public expenditure through the Ministry of Development, General Secretariat of Research and Development, under Measure 8.3 of Operational Programme "Competitiveness" in the Third Community Support Programme.

References

Amiridis, V., D. S. Balis, S. Kazadzis, A. Bais, E. Giannakaki, A. Papayannis, and C. Zerefos (2005), Four-year aerosol observations with a Raman lidar at Thessaloniki, Greece, in the framework of European Aerosol Research Lidar Network (EARLINET), *J. Geophys. Res.*, *110*, D21203, doi:10.1029/2005JD006190.

Balis, D. S., V. Amiridis, S. Nickovic, A. Papayannis, and C. Zerefos (2004), Optical properties of Saharan dust layers as detected by a Raman lidar at Thessaloniki, Greece, *Geophys. Res. Lett.*, *31*, L13104, doi:10.1029/2004GL019881.

Böckmann, C., et al. (2004), Aerosol lidar intercomparison in the framework of the EARLINET project. 2. Aerosol backscatter algorithms, *Appl. Opt.*, *43*(4), 977–989, doi:10.1364/AO.43.000977.

Bohren, C. F., and D. R. Huffman (1983), Absorption and Scattering of Light by Small Particles, John Wiley, Hoboken, N. J.

Bond, T. C., T. L. Anderson, and D. Campbell (1999), Calibration and intercomparison of filter-based measurements of visible light absorption by aerosols, *Aerosol Sci. Technol.*, *30*(6), 582–600, doi:10.1080/027868299304435.

Bösenberg, J., et al. (2003), A European aerosol research lidar network to establish an aerosol climatology, *Report 317*, Max-Planck Inst. fur Meteorol., Hamburg, Germany.

Draxler, R. R., and G. D. Hess (1998), An overview of the HYSPLIT_4 modelling system for trajectories, dispersion and deposition, *Aust. Meteorol. Mag.*, *47*(4), 295–308.

Dubovik, O., and M. D. King (2000), A flexible inversion algorithm for retrieval of aerosol optical properties from Sun and sky radiance measurements, *J. Geophys. Res.*, *105*(D16), 20,673–20,696, doi:10.1029/2000JD900282.

Holben, B. N., et al. (1998), AERONET—A federated instrument network and data archive for aerosol characterization, *Remote Sens. Environ.*, *66*, 1–16, doi:10.1016/S0034-4257(98)00031-5.

Intergovernmental Panel on Climate Change (2007), *Climate Change 2007: The Physical Science Basis, Contribution of Working Group I to the Fourth Assessment Report of the Intergovernmental Panel on Climate Change*, edited by S. Solomon et al., Cambridge Univ. Press, Cambridge, U. K.

Kaufman, Y. J., and R. S. Fraser (1997), The effect of smoke particles on clouds and climate forcing, *Science*, *277*(5332), 1636–1639, doi:10.1126/science.277.5332.1636.

Kazadzis, S., et al. (2007), Nine years of UV aerosol optical depth measurements at Thessaloniki, Greece, *Atmos. Chem. Phys.*, *7*, 2091–2101.

Kelektsoglou, K., S. Rapsomanikis, E. T. Karageorgos, and I. Kosmadakis (2010), Optical properties of aerosol over a south European urban environment, *Int. J. Remote Sens.*, in press.

Matthias, V., et al. (2004), Aerosol lidar intercomparison in the framework of the EARLINET project. 1. Instruments, *Appl. Opt.*, *43*(12), 2578–2579, doi:10.1364/AO.43.002578.

Müller, D., U. Wandinger, and A. Ansmann (1999a), Microphysical particle properties from lidar observations of extinction and backscatter lidar data by inversion with regularization: Theory, *Appl. Opt.*, *37*, 2346–2357, doi:10.1364/AO.38.002346.

Müller, D., U. Wandinger, and A. Ansmann (1999b), Microphysical particle parameters from extinction and backscatter lidar data by inversion with regularization: Simulation, *Appl. Opt.*, *38*, 2358–2368, doi:10.1364/AO.38.002358.

Müller, D., U. Wandinger, D. Althausen, and M. Fiebig (2001), Comprehensive particle characterization from three-wavelength Raman-lidar observations, *Appl. Opt.*, *40*, 4863–4869, doi:10.1364/AO.40.004863.

Müller, D., A. Ansmann, F. Wagner, K. Franke, and D. Althausen (2002), European pollution outbreaks during ACE 2: Microphysical particle properties and single-scattering albedo inferred from multiwavelength lidar observations, *J. Geophys. Res.*, *107*(D15), 4248, doi:10.1029/2001JD001110.

Müller, D., K. Franke, A. Ansmann, D. Althausen, and F. Wagner (2003), Indo-Asian pollution during INDOEX: Microphysical particle properties and single-scattering albedo inferred from multiwavelength lidar observations, *J. Geophys. Res.*, *108*(D19), 4600, doi:10.1029/2003JD003538.

Müller, D., I. Mattis, U. Wandinger, A. Ansmann, D. Althausen, and A. Stohl (2005), Raman lidar observations of aged Siberian and Canadian forest fire smoke in the free troposphere over Germany in 2003: Microphysical particle characterization, *J. Geophys. Res.*, *110*, D17201, doi:10.1029/2004JD005756.

Müller, D., M. Tesche, H. Eichler, R. Engelmann, D. Althausen, A. Ansmann, Y. F. Cheng, Y. H. Zhang, and M. Hu (2006), Strong particle light absorption over the Pearl River Delta (south China) and Beijing (north China) determined from combined Raman lidar and sun photometer observations, *Geophys. Res. Lett.*, *33*, L20811, doi:10.1029/2006GL027196.

Müller, D., A. Ansmann, I. Mattis, M. Tesche, U. Wandinger, D. Althausen, and G. Pisani (2007), Aerosol-type-dependent lidar ratios observed with Raman lidar, *J. Geophys. Res.*, *112*, D16202, doi:10.1029/2006JD008292.

Pahlow, M., D. Müller, M. Tesche, H. Eichler, G. Feingold, W. L. Eberhard, and Y. Cheng (2006), Retrieval of aerosol properties from combined multiwavelength lidar and Sun photometer measurements, *Appl. Opt.*, *45*(28), 7429–7442, doi:10.1364/AO.45.007429.

Pappalardo, G., et al. (2004), Aerosol lidar intercomparison in the framework of the EARLINET project. 3. Raman lidar algorithm for aerosol extinction, backscatter, and lidar ratio, *Appl. Opt.*, *43*(28), 5370–5385, doi:10.1364/AO.43.005370.

Tesche, M., D. Müller, A. Ansmann, M. Hu, and Y. Zhang (2008), Retrieval of microphysical properties of aerosol particles from one-wavelength Raman lidar and multiwavelength sun photometer observations, *Atmos. Environ.*, *42*(25), 6398–6404, doi:10.1016/j.atmosenv.2008.02.014.

Veselovskii, I., A. Kolgotin, V. Griaznov, D. Müller, U. Wandinger, and D. N. Whiteman (2002), Inversion with regularization for the retrieval of tropospheric aerosol parameters from multiwavelength lidar sounding, *Appl. Opt.*, *41*(18), 3685–3699, doi:10.1364/AO.41.003685.

Veselovskii, I., A. Kolgotin, V. Griaznov, D. Müller, K. Franke, and D. N. Whiteman (2004), Inversion of multiwavelength Raman lidar data for retrieval of bimodal aerosol size distribution, *Appl. Opt.*, *43*, 1180–1195, doi:10.1364/AO.43.001180.

V. Amiridis, Institute for Space Applications and Remote Sensing, National Observatory of Athens, 15236 Penteli, Athens, Greece.

A. Bais, D. Balis, and E. Giannakaki, Laboratory of Atmospheric Physics, Aristotle University of Thessaloniki, Campus Box 149, 54124 Thessaloniki, Greece.

K. Kelektsoglou and S. Rapsomanikis, Department of Environmental Engineering, Democritus University of Thrace, PO Box 447, 67100 Xanthi, Greece.

D. Müller, Leibniz Institute for Tropospheric Research, Permoserstr. 15, 04318, Leipzig, Germany.